Supporting Information

Bifunctional Atomically Dispersed Mo-N_2/C Nanosheets Boost Lithium Sulfide Deposition/Decomposition for Stable Lithium-Sulfur Batteries

Feng Ma[†], Yangyang Wan[‡], Xiaoming Wang[§], Xinchao Wang[&], Jiashun Liang[†], Zhengpei Miao[†], Tanyuan Wang[†], Cheng Ma[&], Gang Lu[‡], Jiantao Han[†], Yunhui Huang[†], Qing Li[†, *]

[†]State Key Laboratory of Material Processing and Die & Mould Technology, School of Materials Science and Engineering, Huazhong University of Science and Technology, Wuhan, Hubei 430074, China

[‡]Department of Physics and Astronomy, California State University Northridge, Northridge, California 91330, United States

[§]Department of Chemistry and Key Laboratory for Preparation and Application of Ordered Structural Materials of Guangdong Province, Shantou University, Shantou 515063, China.

[&]Division of Nanomaterials and Chemistry, Hefei National Laboratory for Physical Sciences at the Microscale, CAS Key Laboratory of Materials for Energy Conversion, Department of Materials Science and Engineering, University of Science and Technology of China, Hefei, Anhui 230026, China

*Corresponding Author. E-mail: qing_li@hust.edu.cn (Q. Li)

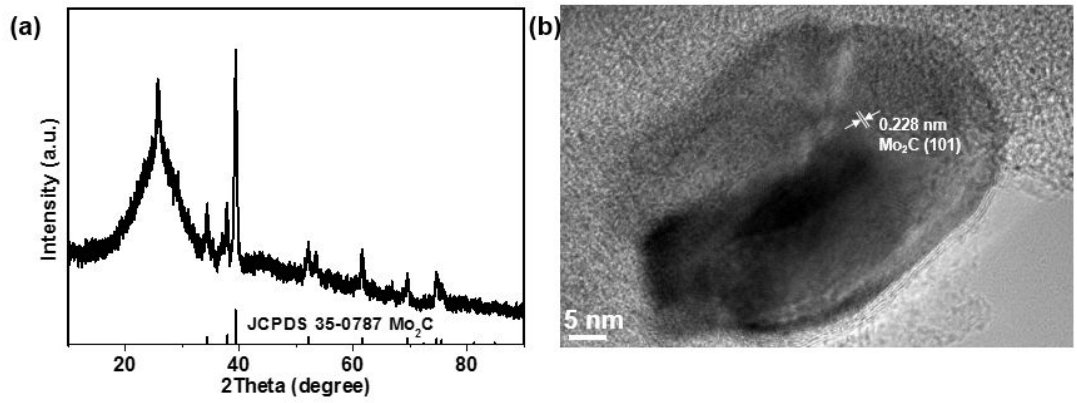

Figure S1. (a) XRD patterns of Mo-N-C-4-900 before acid etching (denoted as Mo-N-C-4-900/Mo_2C); (b) HRTEM image of Mo-N-C-4-900/Mo_2C.

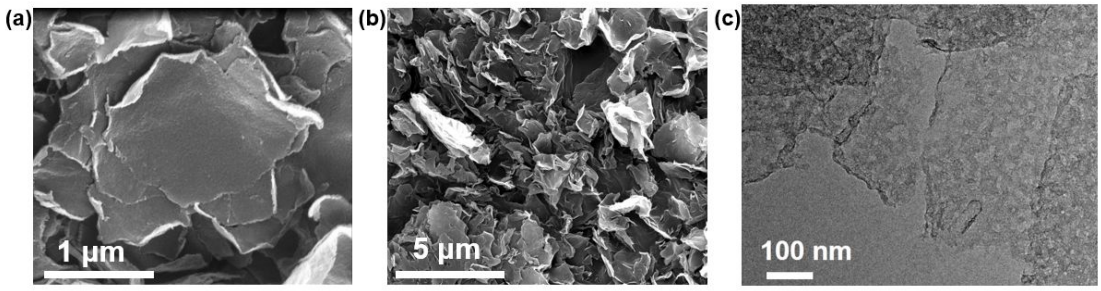

Figure S2. (a-b): SEM with high (a) and low (b) magnification of Mo-N-C-4-900; (c) TEM image of Mo-N-C-4-900.

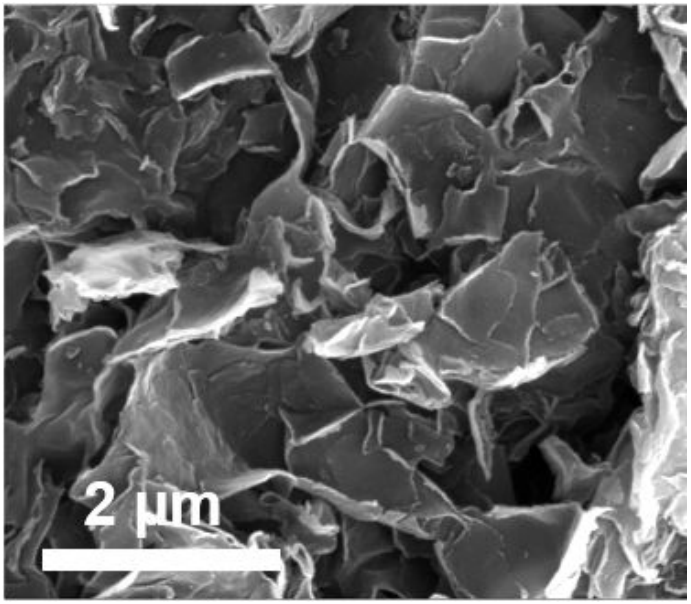

Figure S3. SEM image of N-C.

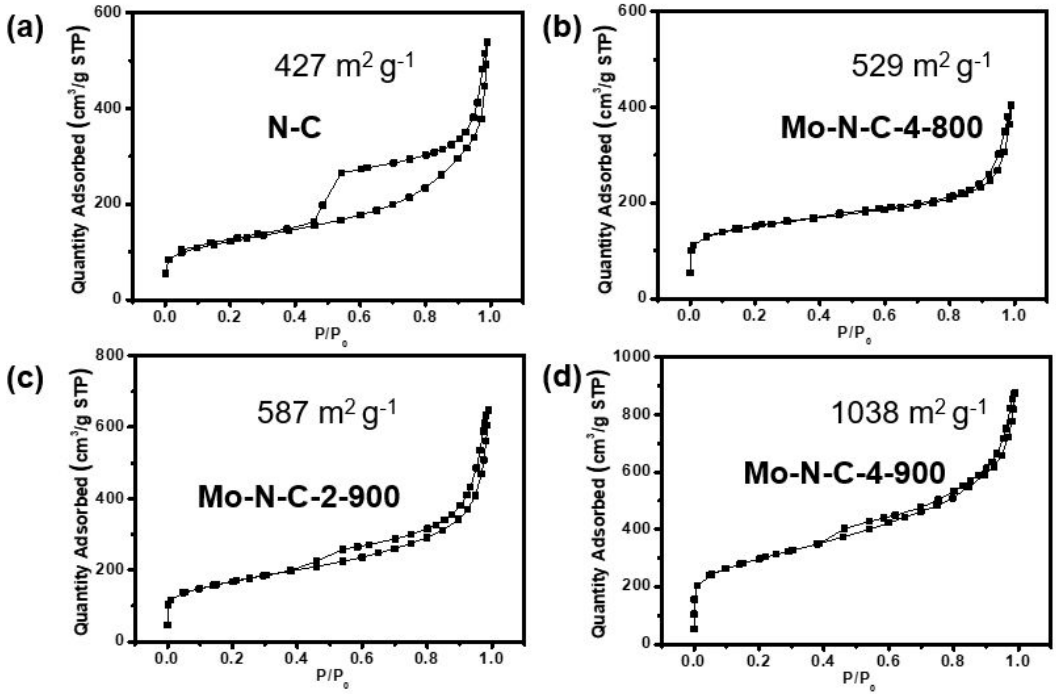

Figure. S4 N_2 adsorption/desorption curves of N-C (a), Mo-N-C-4-800 (b), Mo-N-C-2-900 (c), Mo-N-C-4-900 (d).

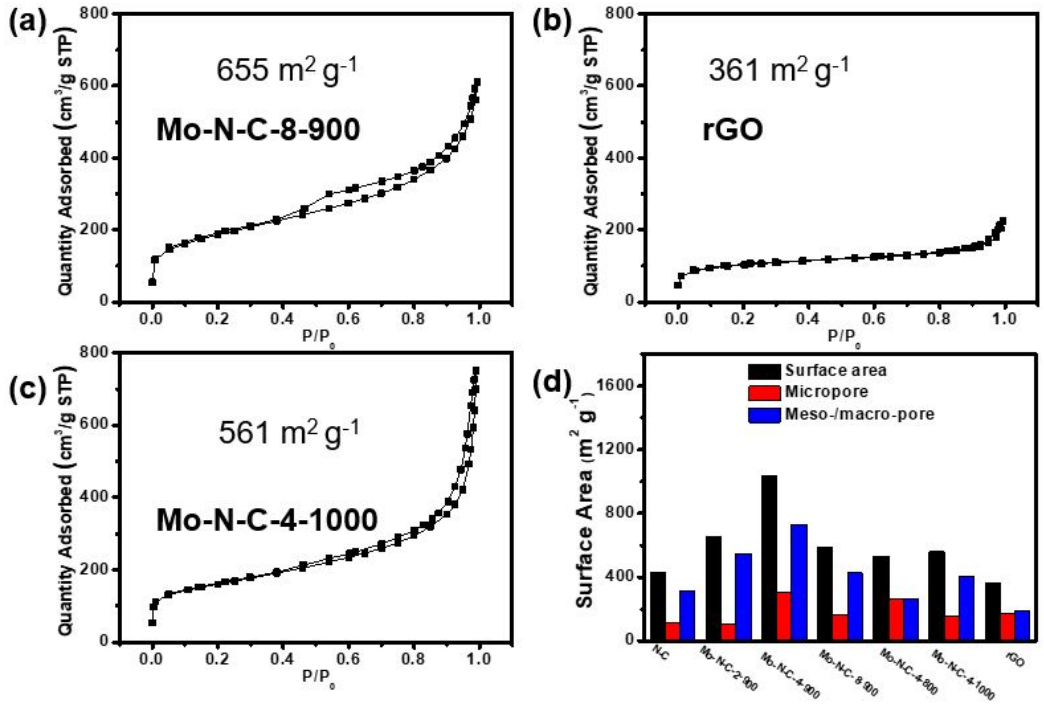

Figure S5. N_2 adsorption/desorption curves of the studied materials: Mo-N-C-8-900 (a), rGO (b), Mo-N-C-4-1000 (c); (d) BET surface areas and pore size distributions of N-C, Mo-N-C-4-900, Mo-N-C-2-900, Mo-N-C-8-900, Mo-N-C-4-800, Mo-N-C-4-1000, and rGO.

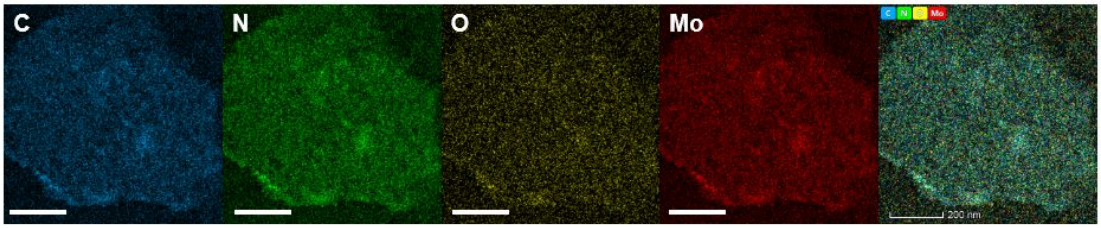

Figure S6. EDS elemental mapping of C (blue), N (green), O (yellow), and Mo (red) for as-prepared Mo-N-C-4-900.

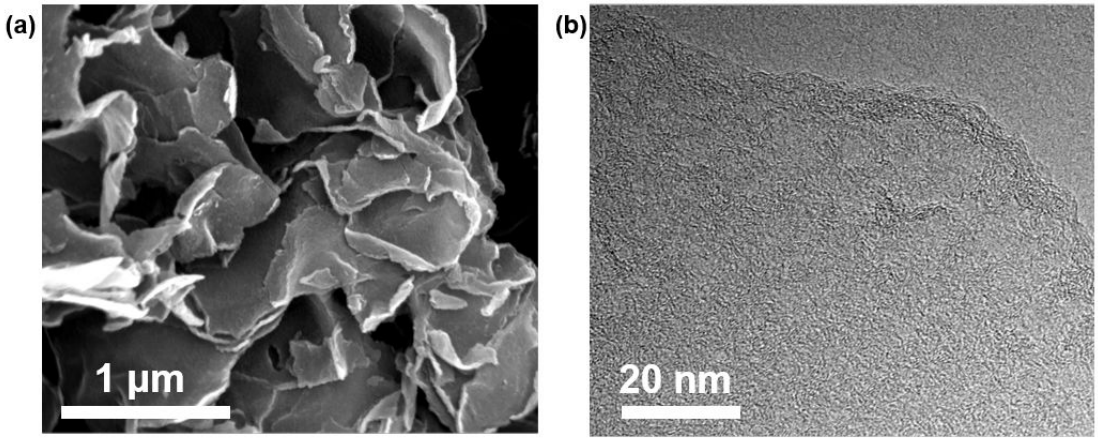

Figure S7. SEM (a) and TEM (b) images of Mo-N-C-8-900.

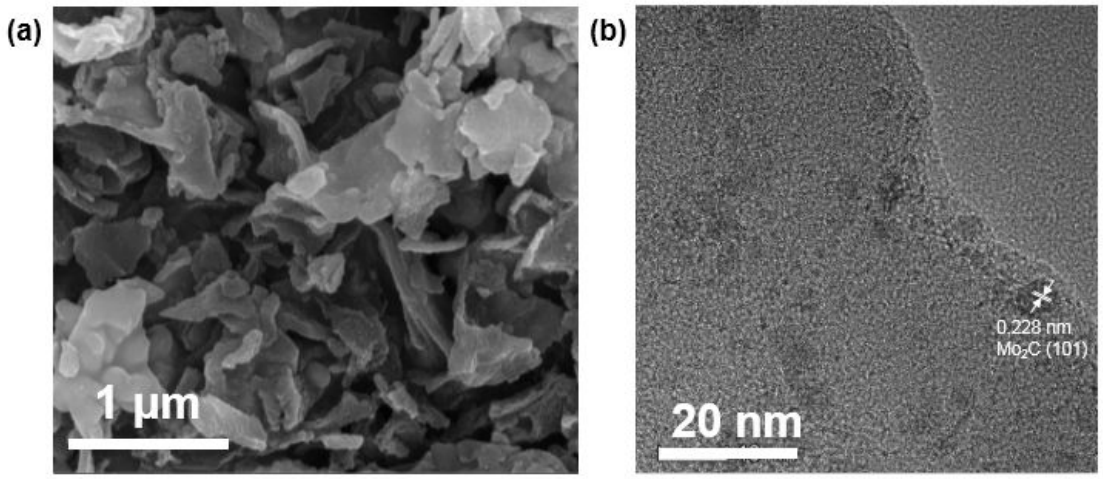

Figure S8. SEM (a) and TEM (b) images of Mo-N-C-2-900.

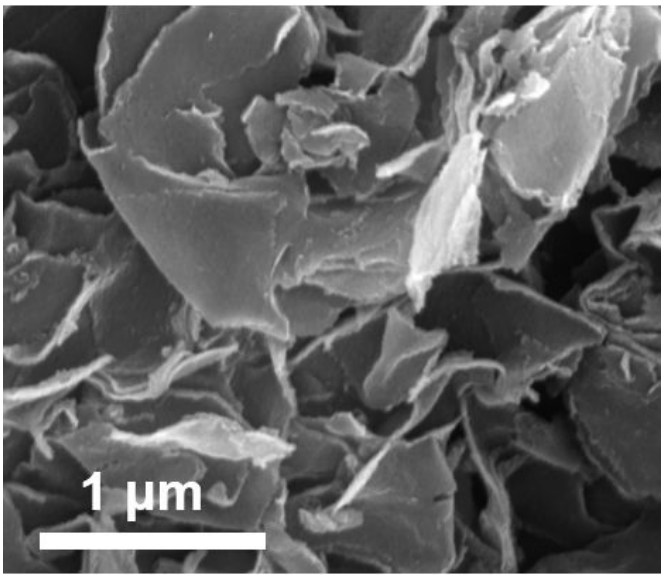

Figure S9. SEM image of Mo-N-C-4-800.

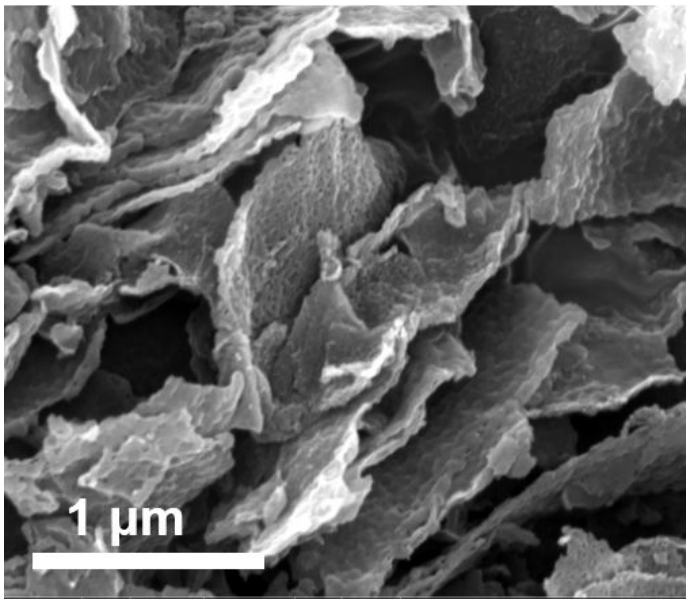

Figure S10. SEM image of Mo-N-C-4-1000.

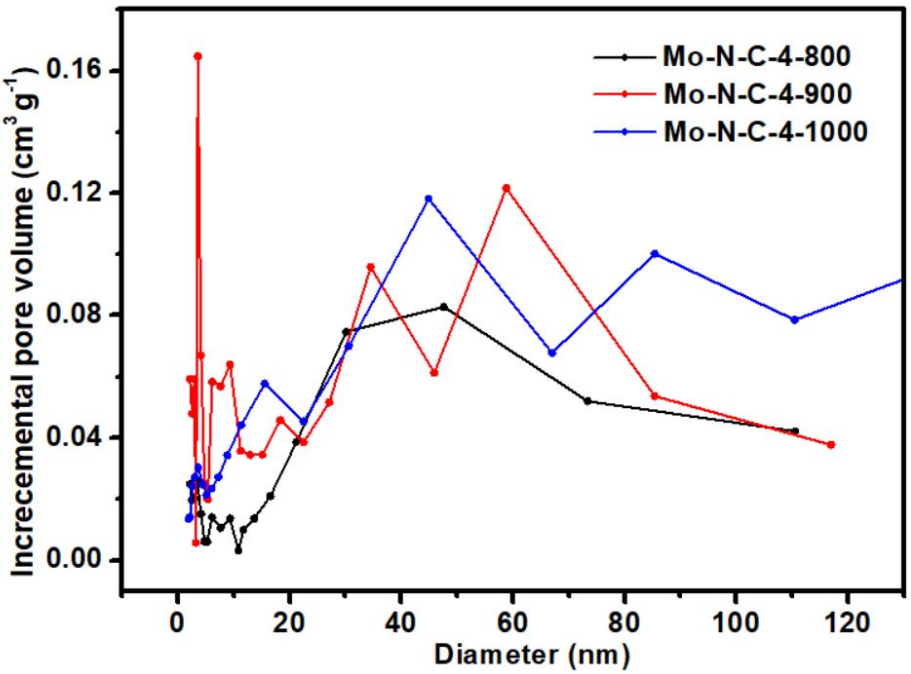

Figure S11. Pore volume distributions of Mo-N-C-4-800, Mo-N-C-4-900, and Mo-N-C-4-1000.

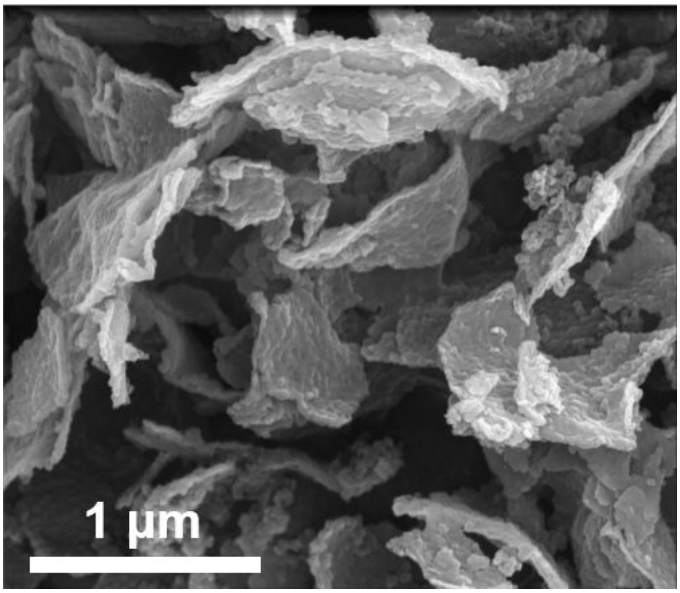

Figure S12. SEM image of S/Mo-N-C-4-900.

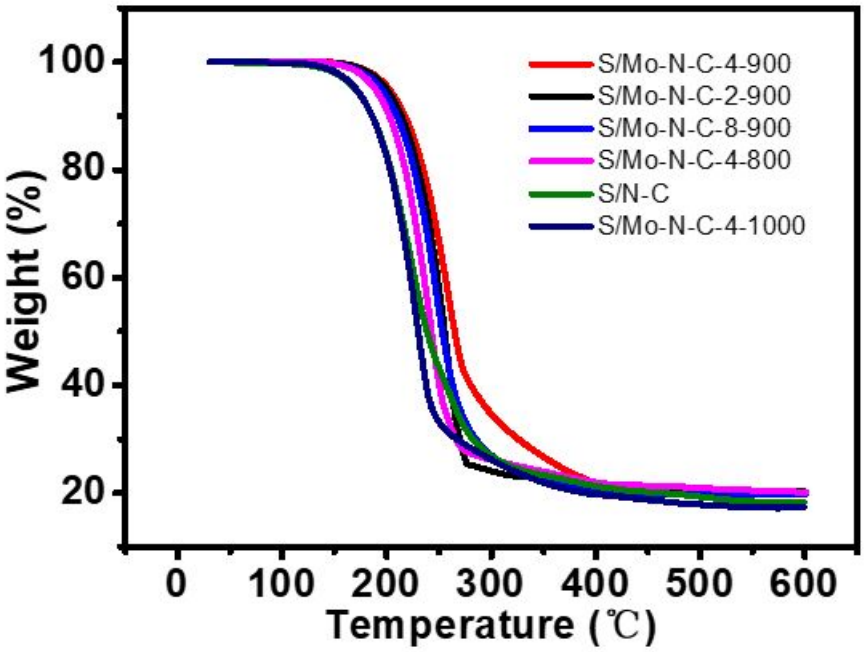

Figure S13. Thermal gravity curves of S/Mo-N-C-4-900, S/Mo-N-C-2-900, S/Mo-N-C-8-900, S/Mo-N-C-4-800, S/Mo-N-C-4-1000, and S/N-C.

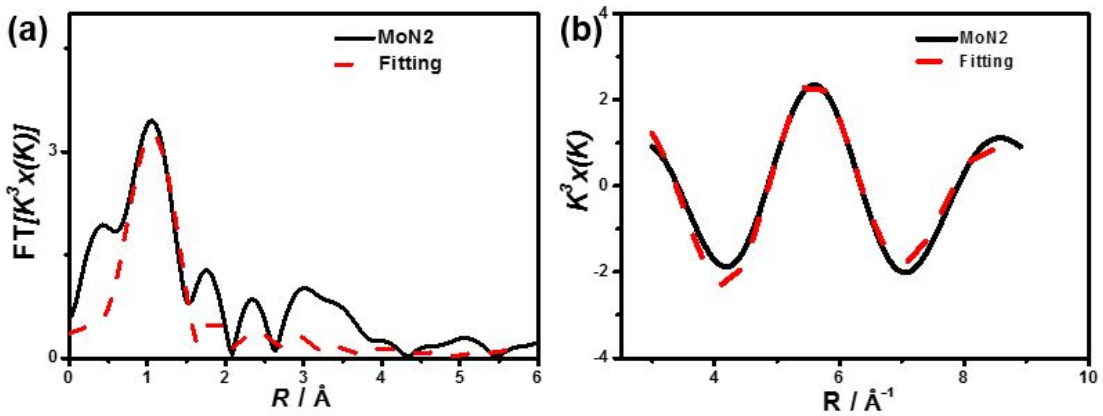

Figure S14. (a) k^3-weighted FT-EXAFS spectrum of Mo-N-C-4-900. (b) The corresponding k^3-weighted EXAFS *r* space fitting curves of Mo-N-C-4-900.

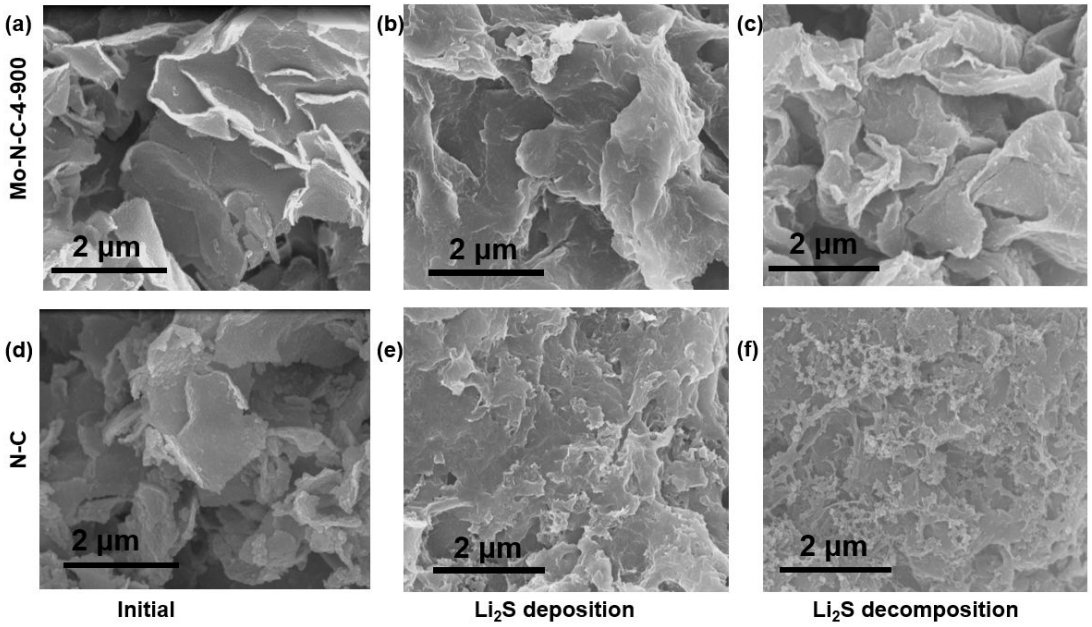

Figure S15. SEM images of Mo-N-C-4-900 (a, b, c) and N-C (d, e, f) in different states: initially (a, d); after Li_2S deposition (b, e); after subsequent Li_2S decomposition (c, f).

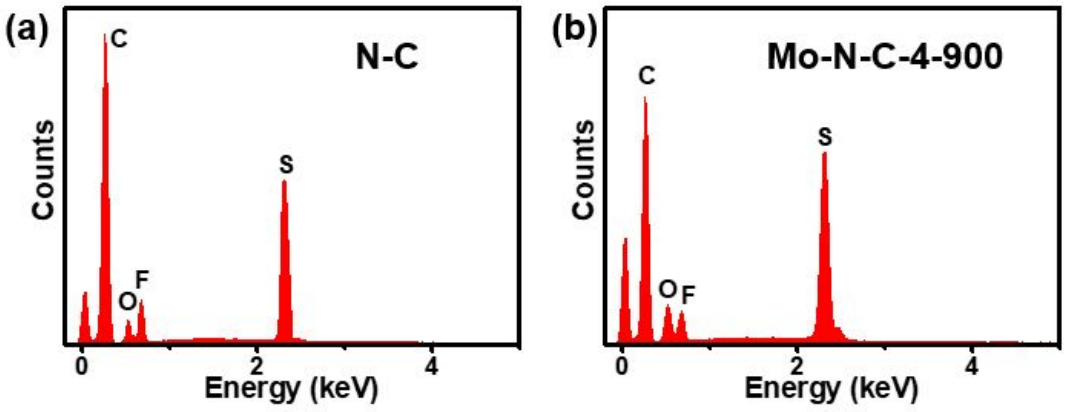

Figure S16. EDS spectra of N-C (a) and Mo-N-C-4-900 (b) electrodes after Li_2S deposition and subsequent Li_2S decomposition measurements.

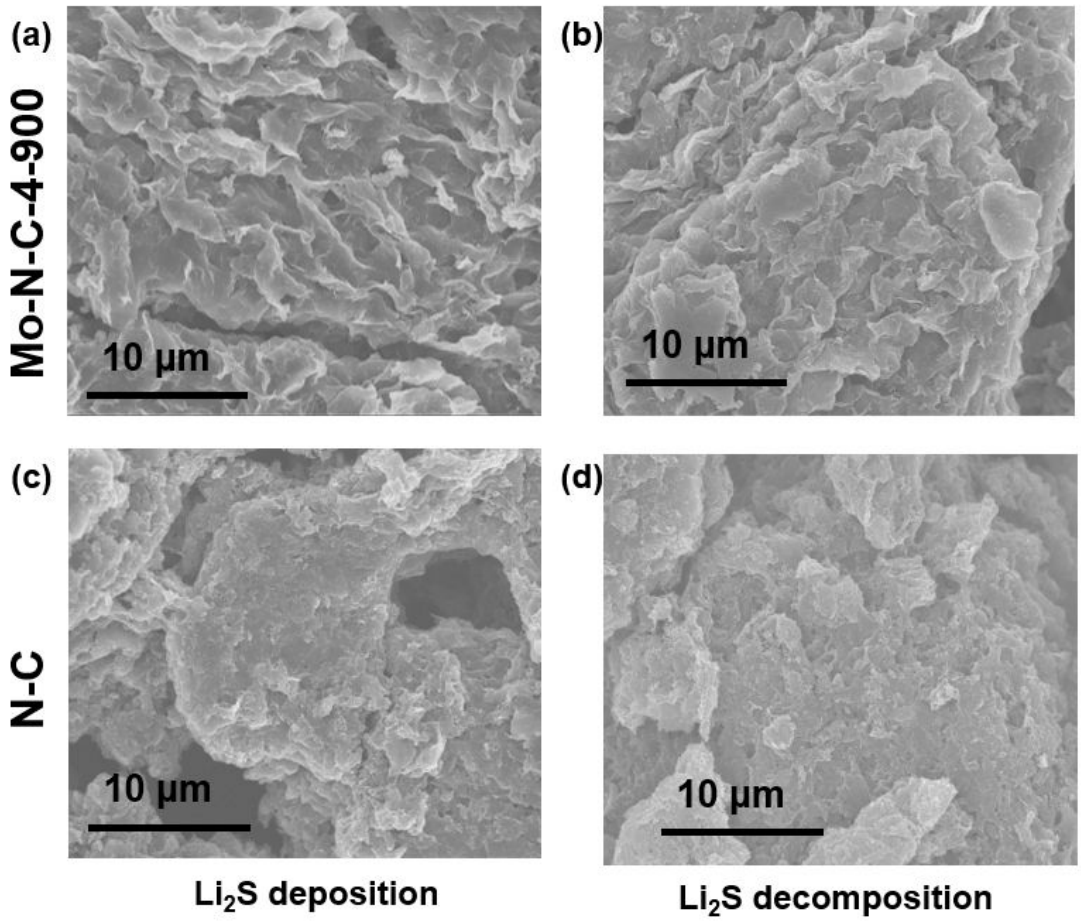

Figure S17. SEM images of Mo-N-C-4-900 (a, b) and N-C (c, d) with lower magnification in different states: after Li_2S deposition (a, c); after subsequent Li_2S decomposition (b, d).

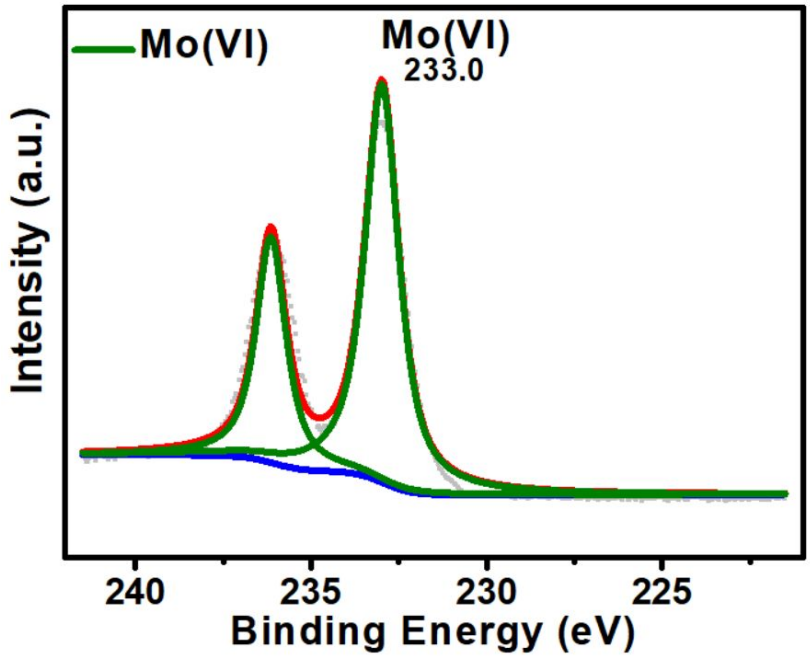

Figure S18. High resolution Mo 3d XPS spectrum of Mo-N-C-4-900 after Li_2S decomposition measurement.

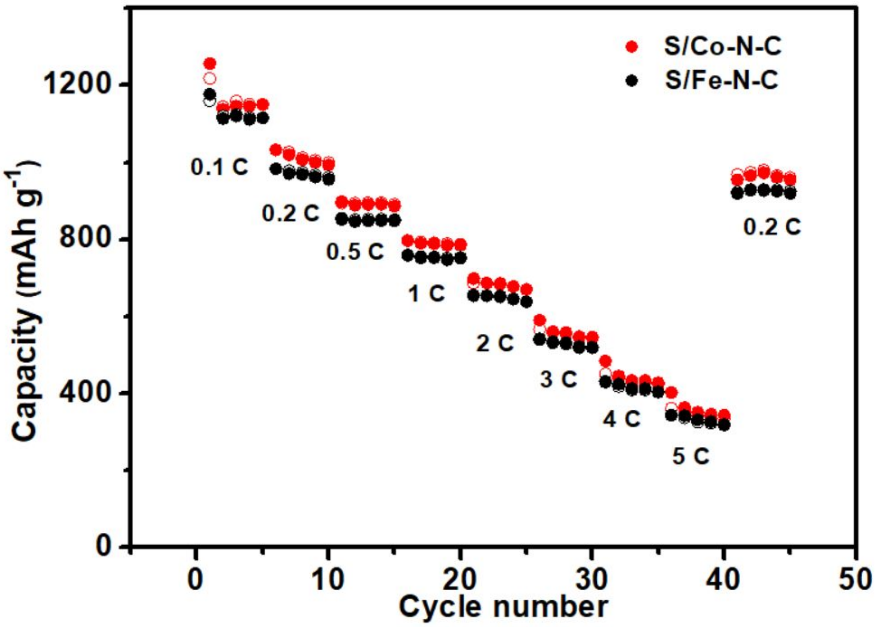

Figure S19. The rate performance of S/Co-N-C and S/Fe-N-C.

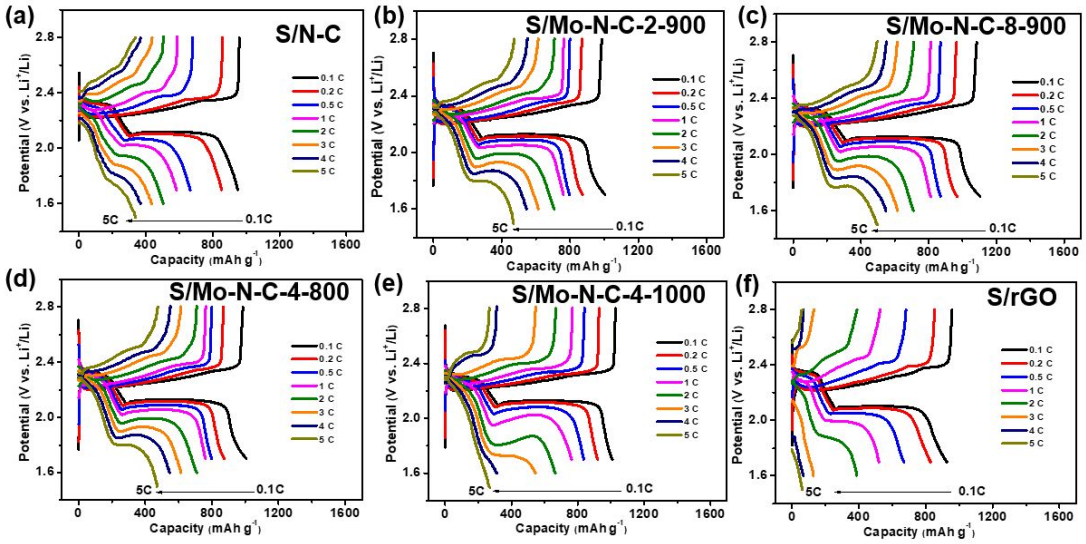

Figure S20. Discharge/charge profiles of S/N-C (a), S/Mo-N-C-8-900 (b), S/Mo-N-C-2-900 (c), S/Mo-N-C-4-800 (d), S/Mo-N-C-4-1000 (e), and S/rGO (f) under constant current densities from 0.1 C to 5 C.

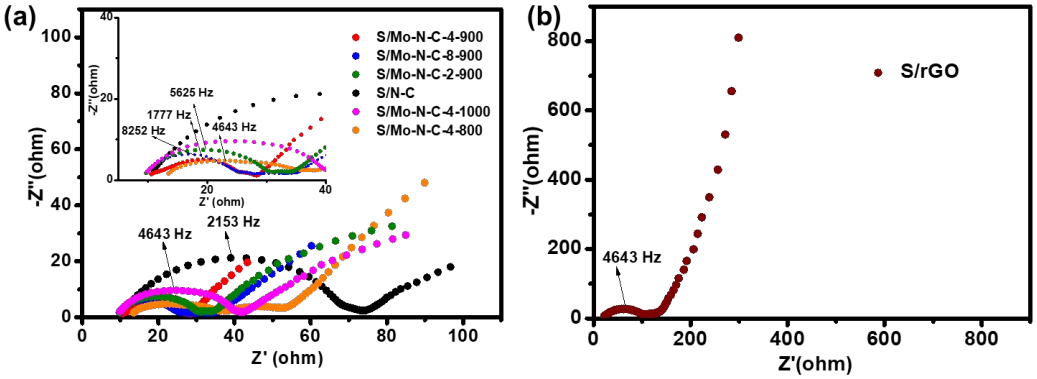

Figure S21. EIS plots of (a) S/N-C, S/Mo-N-C-4-900, S/Mo-N-C-2-900, S/Mo-N-C-8-900, S/Mo-N-C-4-800, S/Mo-N-C-4-1000, and (b) S/rGO. The insert in (a) shows the magnification of the high and medium frequency region of the plots

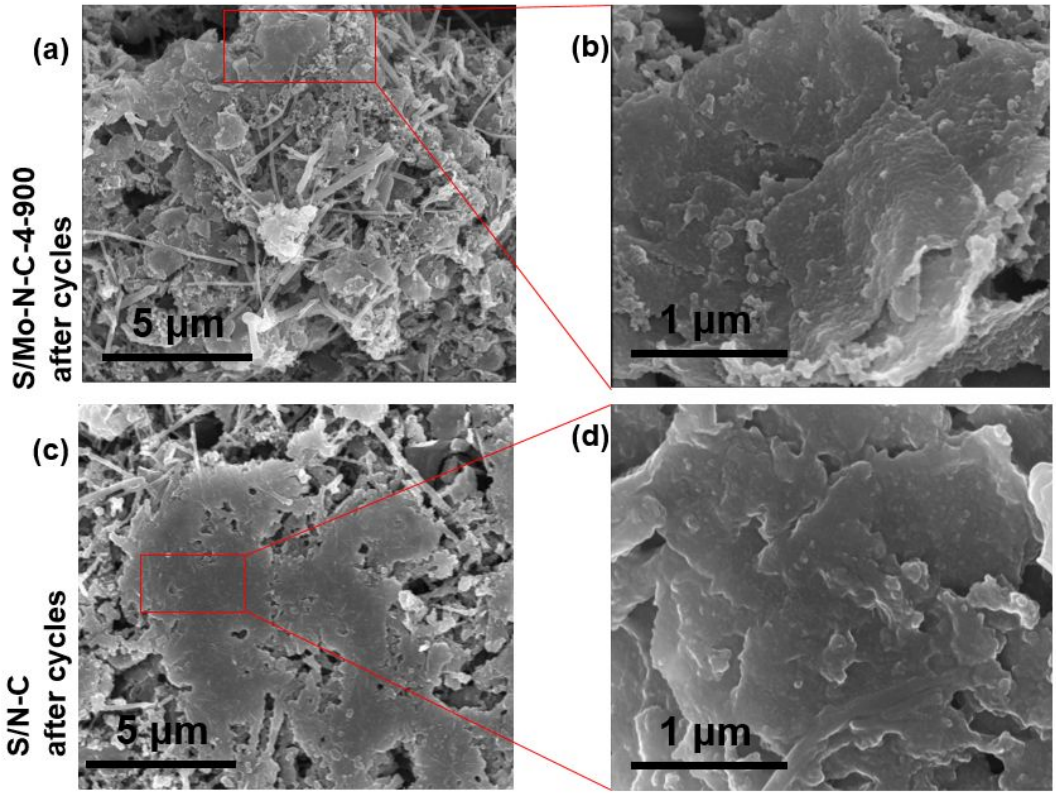

Figure S22. SEM images of S/Mo-N-C-4-900 (a, b) and S/N-C (c, d) after cycling.

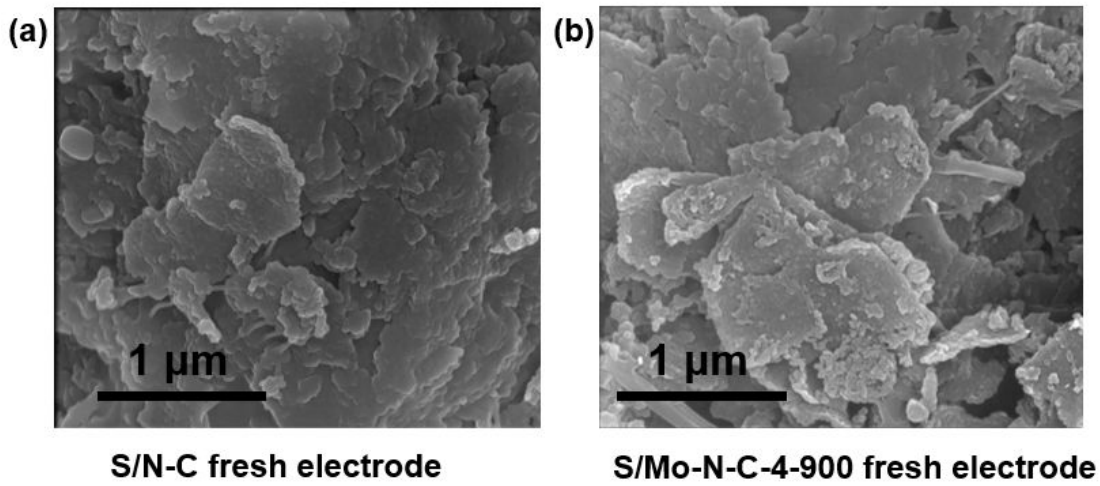

Figure S23. SEM images of S/N-C (a) and S/Mo-N-C-4-900 (b) fresh electrodes.

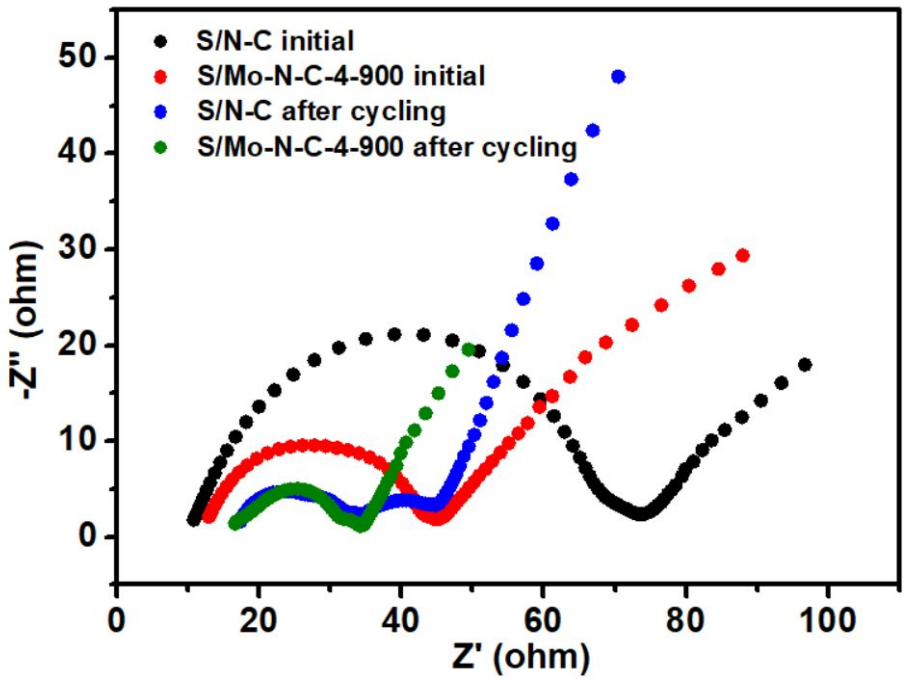

Figure S24. EIS plots of S/Mo-N-C-4-900 and S/N-C before and after cycling.

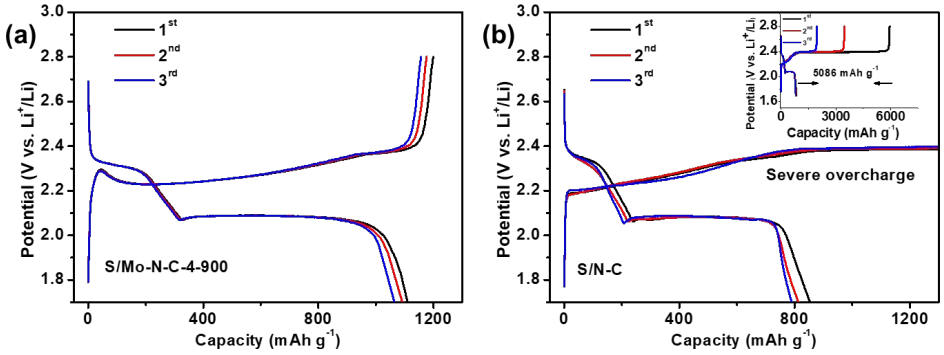

Figure S25. (a-b): The discharge/charge profiles of S/Mo-N-C-4-900 (a) and S/N-C (b) at 0.2 C in the $LiNO_3$-free electrolyte.

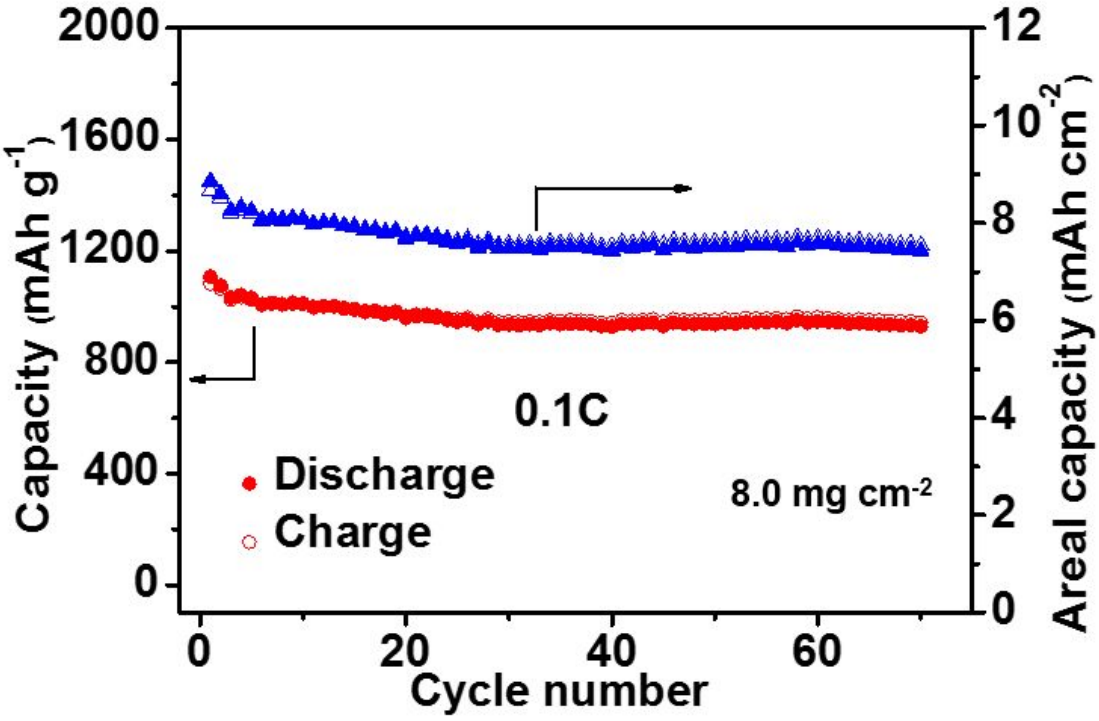

Figure S26. Cycling performance of S/Mo-N-C-4-900 with S loading of 8.0 mg cm^{-2} at 0.1 C.

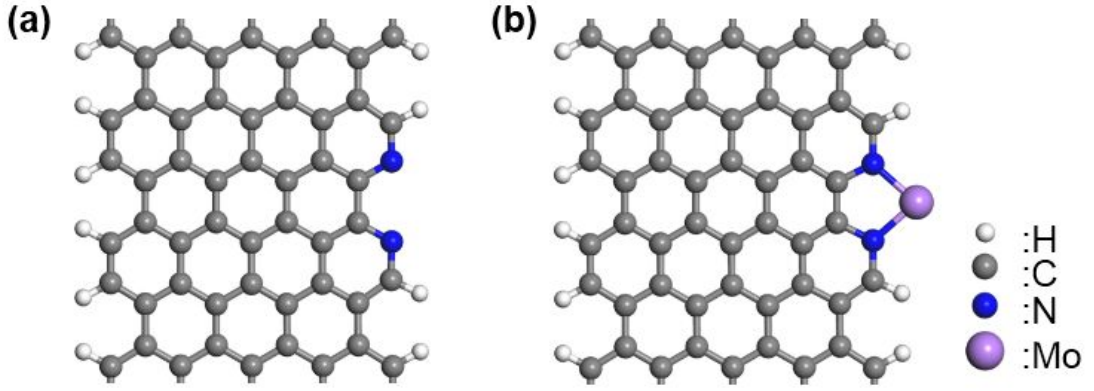

Figure S27. Illustrations of the local structures of N-C (a) and Mo-N-C-4-900 (b) used in DFT calculation.

Table S1. the Mo content in Mo-N-C-4-900, Mo-N-C-2-900, and Mo-N-C-8-900 based on XPS results.

Samples	Mo content
Mo-N-C-4-900	0.36 at%
Mo-N-C-2-900	0.93 at%
Mo-N-C-8-900	0.25 at%

Table S2. Mo K-edge EXAFS curve fitting parameters of Mo-N-C-4-900.

Pairs	Coordination number	Bond distance	dE	Debye-wallor factor	Residue
Mo-N	2.251±0.193	1.440±0.008	6.047	0.111±0.013	1.231

Table S3. Summary of performance of molybdenum compounds and M-N-C in Li-S batteries

Materials	Sulfur Content	Rate Capability (mAh g^{-1})	Capacity Retention	Ref.
Mo_2C–C NOs	72.15 wt% 1.1 mg cm^{-2}	1398 mAh g^{-1} (0.1 C) 337 mAh g^{-1} (5 C)	72.58% (600 cycles at 1 C)	1
MoS_{2-x}/rGO	75 wt%	1310.5 mAh g^{-1} (0.1 C) 826.5 mAh g^{-1} (8 C)	50.2% (600 cycles at 0.5 C)	2
Mo-80S	80.2 wt%	1250 mAh g^{-1} (0.1 C) 788 mAh g^{-1} (5 C)	ca. 75% (100 cycles at 5 C)	3
Fe-N-C/S-MCF	60 wt% 2.5 mg cm^{-2}	1244 mAh g^{-1} (0.1 C) 798 mAh g^{-1} (5 C)	68.9% (100 cycles at 0.5 C)	4
Fe-PNC	70 wt% 1.3 mg cm^{-2}	1138.6 mAh g^{-1} (0.1 C) ca. 280 mAh g^{-1} (2 C)	40% (300 cycles at 0.1 C)	5
Co-N/G	90 wt% 2.0 mg cm^{-2}	1210 mAh g^{-1} (0.2 C) 618 mAh g^{-1} (4 C)	73.5% (500 cycles at 1 C)	6
Ni@NG*	ca. 2.5 mg cm^{-2}	1598 mAh g^{-1} (0.1 C) 612 mAh g^{-1} (10 C)	78% (500 cycles at 1 C)	7
Li_2S@NC:SAFe**	ca. 66.4 wt% 1.39-1.6 mg cm^{-2}	ca. 1200 mAh g^{-1} (0.2 C) 589 mAh g^{-1}(12 C)	60% (1000 cycles at 2 C)	8
Mo-N-C	**81 wt%** **2.0 mg cm^{-2}**	**1360.2 mAh g^{-1}(0.1 C)** **743.9 mAh g^{-1}(5 C)**	**90% (550 cycles at 2 C)**	**This work**

*** Ni@NG** was used as functional separator in the Li-S battery with Li_2S_6-containing electrolyte as the S source.

** A super aligned carbon nanotube film was placed on the surface of Li_2S@NC:SAFe electrode in Li-S battery, and the S content is normalized based on the Li_2S content mentioned in the literature.

(1) Chen, G.; Li, Y.; Zhong, W.; Zheng, F.; Hu, J.; Ji, X.; Liu, W.; Yang, C.; Lin, Z.; Liu, M., MOFs-Derived Porous Mo_2C–C Nano-Octahedrons Enable High-Performance Lithium–Sulfur Batteries. *Energy Storage Mater.* **2020,** *25*, 547-554.

(2) Lin, H. B.; Yang, L. Q.; Jiang, X.; Li, G. C.; Zhang, T. R.; Yao, Q. F.; Zheng, G. W.; Lee, J. Y., Electrocatalysis of Polysulfide Conversion by Sulfur-Deficient MoS_2 Nanoflakes for Lithium-Sulfur Batteries. *Energy Environ. Sci.* **2017,** *10*, 1476-1486.

(3) Liu, X. C.; Zhou, S. P.; Liu, M.; Xu, G. L.; Zhou, X. D.; Huang, L.; Sun, S. G.; Amine, K.; Ke, F. S., Utilizing A Metal as A Sulfur Host for High Performance Li-S Batteries. *Nano Energy* **2018,** *50*, 685-690.

(4) Lim, W. G.; Mun, Y.; Cho, A.; Jo, C. S.; Lee, S.; Han, J. W.; Lee, J., Synergistic Effect of Molecular-Type Electrocatalysts with Ultrahigh Pore Volume Carbon Microspheres for Lithium-Sulfur Batteries. *ACS Nano* **2018,** *12*, 6013-6022.

(5) Liu, Z. Z.; Zhou, L.; Ge, Q.; Chen, R. J.; Ni, M.; Utetiwabo, W.; Zhang, X. L.; Yang, W., Atomic Iron Catalysis of Polysulfide Conversion in Lithium-Sulfur Batteries. *ACS Appl. Mater. Interfaces.* **2018,** *10*, 19311-19317.

(6) Du, Z. Z.; Chen, X. J.; Hu, W.; Chuang, C. H.; Xie, S.; Hu, A. J.; Yan, W. S.; Kong, X. H.; Wu, X. J.; Ji, H. X.; Wan, L. J., Cobalt in Nitrogen-Doped Graphene as Single-Atom Catalyst for High-Sulfur Content Lithium-Sulfur Batteries. *J. Am. Chem. Soc.* **2019,** *141*, 3977-3985.

(7) Zhang, L. L.; Liu, D. B.; Muhammad, Z.; Wan, F.; Xie, W.; Wang, Y. J.; Song, L.; Niu, Z. Q.; Chen, J., Single Nickel Atoms on Nitrogen-Doped Graphene Enabling Enhanced Kinetics of Lithium-Sulfur Batteries. *Adv. Mater.* **2019,** *31*, 1903955.

(8) Wang, J.; Jia, L.; Zhong, J.; Xiao, Q.; Wang, C.; Zang, K.; Liu, H.; Zheng, H.; Luo, J.; Yang, J.; Fan, H.; Duan, W.; Wu, Y.; Lin, H.; Zhang, Y., Single-Atom Catalyst Boosts Electrochemical Conversion Reactions in Batteries. *Energy Storage Mater.*

2019, *18*, 246-252.